The Behaviour of Plasma-Functionalized Graphene Nanoflake Nanofluids during Phase Change from Liquid Water to Solid Ice

*Adam McElligott, Alex Whalen, Chong Yang Du, Lukas Näveke, Jean-Luc Meunier, Phillip Servio**

Department of Chemical Engineering, McGill University, Montreal, Quebec H3A 0C5, Canada

ABSTRACT

Emerging nanofluid-based technologies for cooling, transport, and storage applications have previously been enhanced through the use of graphene nanoflake (GNF) nanofluids. Many of the beneficial effects of GNFs have now been documented, though little work has yet been completed to characterize the morphological behaviour of GNF nanofluids both during and after the phase change process. In this study, the crystallization behaviour of sessile water droplets was evaluated for two plasma-functionalized, hydrophilic GNF concentrations (20 and 100 ppm) at three driving force temperatures (-5, -10, and -20 °C). At low driving forces, the GNFs were wholly expelled from the solid matrix due to low crystallization velocities. At high driving forces, more rapid crystallization rates resulted in the entrapment of GNFs within the air bubbles and inter-dendritic spaces of the solid droplet. However, individual particle dispersion was not achieved within the

solid matrix at any driving force. Furthermore, for all experimental conditions, the functionalized GNF clusters which formed during freezing did not disperse spontaneously upon melting as drying-like effects may have altered the attraction properties of their surfaces and destabilized the suspension. Compared to previous studies using MWCNTs, the GNFs were found to have higher liquid mobility at the solid front, provide less resistance to that front as it ascended, and be better dispersed after melting. These effects may have been geometrical; the square nanoflake geometry does not result in any physical particle entanglement.

INTRODUCTION

A nanofluid is a stable suspension of nanometer-sized particles (nanoparticles) in a host fluid.[1] These biphasic systems are often colloidal as the solid phase is homogeneously dispersed within the liquid phase.[2] The settling of these particles is avoided due to Brownian motion, which results from their minute scale, prevailing over gravitational forces.[3] The presence of nanoparticles, which have high surface area to volume ratios, has been shown to introduce new desirable properties to the host fluid. These properties have primarily included enhanced heat and mass transport, gas absorption, and electrical conductivity, though, more recently, magnetic and tunable optical properties have been explored as well.[3] These findings have led to a surge in studies of nanofluids, investigating a wide array of applications that could benefit from enhanced fluid properties.

Graphene nanosheets or nanoflakes (GNFs) are a particular class of carbon nanoparticle that consist of layers of highly-crystalline graphitic sheets with a low defect concentration.[4] GNFs have high electrical and thermal conductivities, superior mechanical strength, and have been found to enhance transport properties when in a nanofluid.[4-6] The performance of nanofluids is highly dependent on a well-maintained homogeneous dispersion of particles in the solution. Therefore, the main challenge with GNF-based nanofluids is that their carbon content results in a hydrophobic

nature and thus an unstable nanofluid. To overcome attractive van der Waals forces, appropriate techniques are required to ensure homogeneous dispersion in polar solvents. Stable suspensions can be attained through numerous approaches, the most common of which are the addition of surfactants to GNF-containing systems and direct chemical surface modification of the GNFs.[2] The addition of surfactant molecules can be both economical and practical; however, the robustness of the additives themselves is not always sufficient, and their presence may alter the desired nanofluid properties. The functionalization of GNF surfaces is a more appropriate approach and can be achieved through wet or dry methods. The functionalization process aims to fix polar functional groups to the particle surface, rendering the nanoflakes hydrophilic and resulting in a stable suspension.[4] The presence of oxygenated GNFs (O-GNFs) in a polar solvent likely causes deprotonation of the oxygen groups and leads to the formation of an electrostatic double layer around the particles.[3] As outlined in DLVO theory, repulsive Coulombic forces between similarly charged particles then uphold GNF dispersion.[7] Surface functionalization methods can be more costly and technically involved, but avoid the addition of a ternary component to the system. These methods, along with the robustness of the GNFs, allow for a reliable, effective evaluation of the nanomaterial's properties and effects on a system.[3] Recent advances in GNF functionalization techniques have permitted surface functionalization through plasma treatment.[4] This technique is simple as it requires less chemical reactants, which in turn reduces cost and material waste. Moreover, it produces consistent, homogeneous nanofluids that are stable over extended periods and at temperatures significantly higher than the limit for surfactants.[4]

Carbon nanofluids have been previously investigated for their improved conductive and convective heat transfer properties.[2] The discovery of these effects led to a new branch of nanofluid

studies which has been focusing on phase change enhancement of the base fluid, most commonly for liquid-to-solid transitions. Some examples of applications that are currently exploring this phenomenon are cool thermal energy storage (CTES), cryopreservation, and gas hydrate formation.[3, 8-11] These phase change studies are essential as analyses pertaining specifically to the phase change behaviour of colloidal systems have critical implications on the feasibility of these emerging technologies. Carbon nanofluids have been shown to facilitate nucleation in liquid-to-solid systems.[11] These nanofluids increase the efficiency of phase change processes as less energy is required to form the new phase. Furthermore, carbon nanofluids have been shown to enhance sensible cooling and solidification rates, as well as the total amount of liquid-to-solid conversion.[10-14] A narrow focus was placed on using MWCNTs (multi-walled carbon nanotubes) as the nanoparticle of interest in these studies, meaning GNF effects are relatively uncharacterized. However, GNF nanofluids are of high interest as they may offer superior properties when compared to other nanofluids in phase change systems. Specifically for energy transport applications, GNF solutions have been found to increase the mass diffusivity of methane during the formation of a gas hydrate phase significantly more than MWCNTs.[8, 15] However, the characteristics of GNFs during and after freezing processes are yet to be analyzed, which is essential in further assessing the hydrate-promoting mechanism. Furthermore, the impact of crystallization on GNFs may provide a more comprehensive understanding regarding the feasibility of implementing upcoming nanofluid-based technologies since the stability of these fluids is vital to their performance.

The water to ice phase change process, which is a heat transport process, is often divided into three different kinetic stages.[16] These stages are outlined in Figure 1, where stage 0 is a water droplet at rest. The first stage is the rapid growth of a small expanse of crystal into the liquid bulk.

This typically dendritic growth immediately follows nucleation, and its extent becomes more substantial as supercooling increases. As this growth occurs in the order of seconds, the growth rate is often self-limited because of the rise in temperature of the surrounding fluid caused by the significant amount of heat released from the exothermic crystallization process.[17-18] In the second stage, the remaining bulk of the droplet is converted from a liquid into a solid over several minutes. This solidification stage is limited by the speed at which the latent heat of crystallization is transferred from the liquid at the solid interface to the medium surrounding it (i.e., heat conduction).[17, 19] The third and final step is the correction of imperfections in the crystal matrix through solid-state adjustments. This process can progress over hours to days[16, 20], and is beyond the timescales considered in this study.

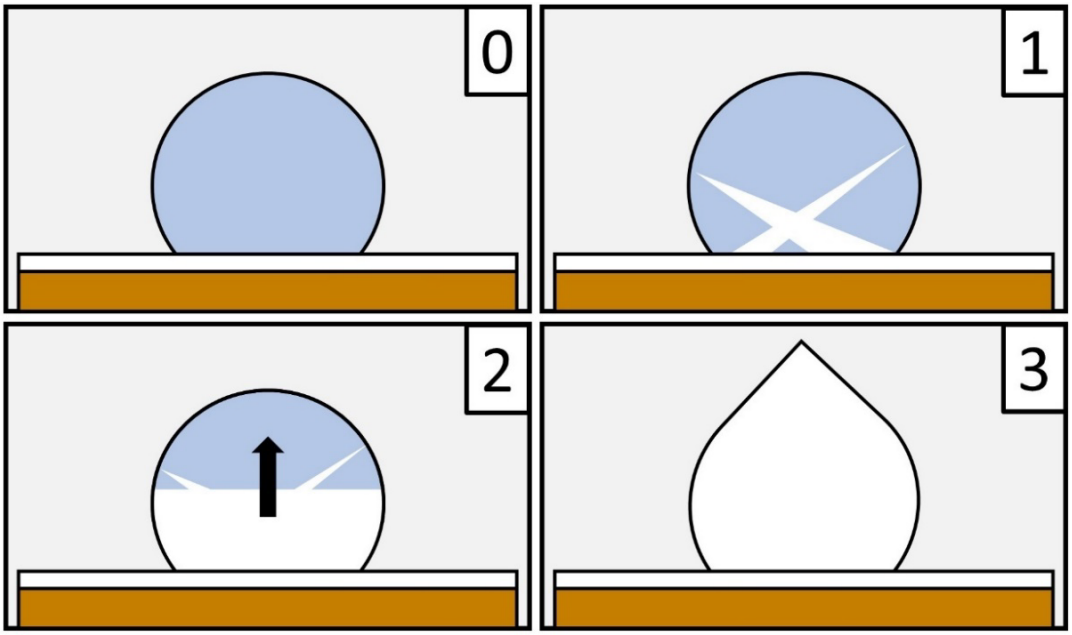

Figure 1. Kinetic Stages of Phase Change: Initial (0), Dendritic Growth (1), Planar Growth (2), Solid-State Adjustments (3)

In this study, the solidification behaviour of static droplets made of aqueous suspensions of oxygen-functionalized GNFs is investigated through morphological analysis. Water is chosen as

the base medium as it is a conventional fluid for suspensions, and the study of its crystallization has many industrial and practical applications. The effects of two O-GNF concentrations and three driving force temperatures are evaluated, and the visual characteristics of the nanofluid after melting are detailed and analyzed. To the best of our knowledge, this is the first study to investigate the crystallization morphology of hydrophilic graphene nanofluids and to characterize the nanofluid behaviour at different levels of supercooling, as well as after the melting process.

MATERIALS AND METHODS

A full schematic of the experimental apparatus described below is provided in Figure 2. The thermoelectric (TE) cooler module (TE Technology) consists of a Peltier cold plate (CP-200TT) connected to both a temperature controller (TC-36-25) and a power supply. A general-purpose thermistor (MP-3193, tolerance of ± 1.0 °C between 0 and 70 °C, +1.4/-2.2 °C at -20 °C) with an operating range of -20 to 100 °C is used to monitor cold plate temperature. A LabVIEW^{TM} Virtual Instrument is used to set controller parameters and record data. Images are taken with a Canon EOS 60D DSLR camera (18.0-megapixel CMOS sensor) equipped with an MP-E 65 mm f/2.8 1-5x macro lens. This camera is mounted onto an OptoSigma multi-axis manual positioner stage used to fine-tune the camera's focal point. The camera is angled, pointing just slightly down but nearly normal to the droplet (exaggerated in the figure) for optimal visualization of the solid front and is approximately parallel to the surface of the cold plate. To illuminate the droplet, a Schott KL 2500 fibre optic LED set to 50% intensity is used along with a white reflective screen to improve brightness. The screen is placed behind the sample and fixed to the Styrofoam insulation. This insulation is on top of the cold plate, covering the entire surface except for the area on which the sample is placed. A weighted lid of the same material is also placed above the sample to

improve condition consistency during data acquisition. The entire apparatus is mounted onto a Newport RS 3000 optical table to reduce potential vibrations.

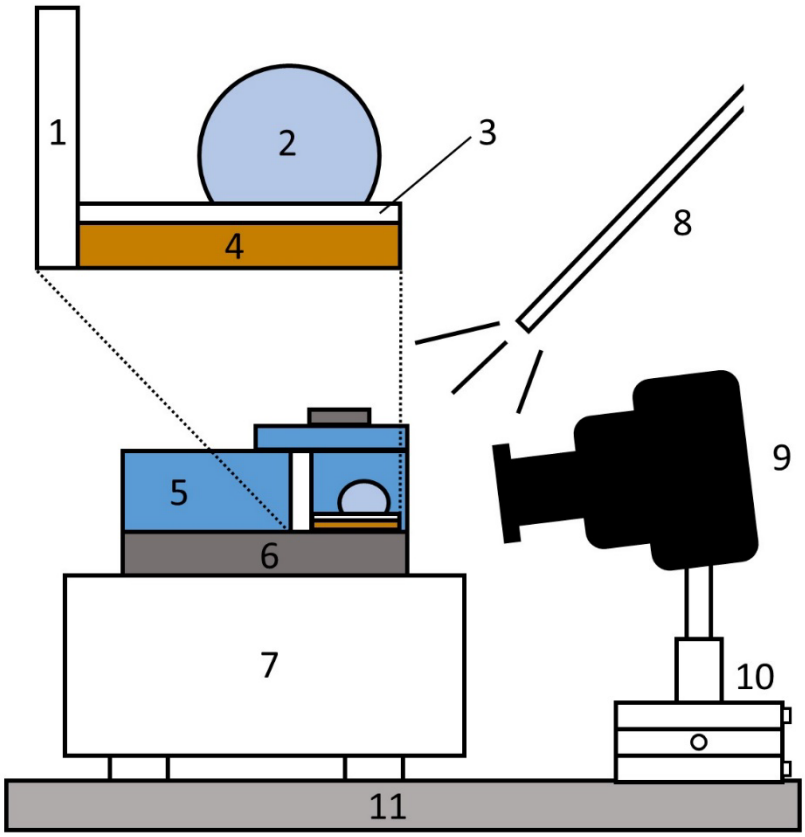

Figure 2. Experimental Apparatus Cross Section Schematic. Includes reflective surface (1), liquid droplet (2), PTFE strip (3), copper plate (4), Styrofoam insulation with weighted lid (5), TE cold plate surface (6), TE cold plate body (7), LED light source (8), camera with lens (9), multi-axis manual positioner (10), and optical table (11)

A two-stage process is used to produce oxygen-functionalized GNFs (O-GNFs). The first stage is a homogeneous nucleation process wherein critical carbon clusters form from carbon vapours. This process is typically performed in a temperature window between 4000 and 5000 K within the thermal plasma reactor.[4] The carbon clusters grow only in 2-dimensions due to a control of the temperature, flow, and nucleation fields. As a result, a pure powder of graphene sheets is formed,

the bulk of which is deposited inside the thermal plasma reactor on a collecting plate. The methane/nitrogen gas feed is changed to air (oxygen/nitrogen) in the second stage of the process in order to generate oxygen functional groups on the carbon nanoparticles. The oxygen in the air forms an active species that interacts with the surface of the GNF, which produces a tunable quantity of hydrophilic groups.[4] Both hydrophobic and hydrophilic GNFs have in-plane dimensions of roughly 100 x 100 nm^2 and are ten atomic layers thick on average. Through XPS (x-ray photoelectron spectroscopy) on the O-GNF, zeta potential measurements as well as nanofluid stability tests, it was determined that a stable nanofluid showing no agglomeration over several months was obtained when the atomic composition reached approximately 14.2 at% oxygen.[4] The presence of C–O, C=O, and O=C–O bonds was found through the deconvolution of the oxygen and carbon XPS peaks. These bonds correspond to hydrophilic groups such as esters, carboxylic acids, anhydrides, hydroxides, and ether oxides.[4] The hydrophobic GNFs do not mix in the presence of water, while the hydrophilic GNFs become perfectly dispersed in water without a surfactant present.[4] While there was no visual evidence of agglomeration, the O-GNF solutions were made several months prior to experimentation and thus were ultrasonicated in a Branson 2510 ultrasonic cleaner (a sonicating bath) to ensure dispersion. Further information regarding production, functionalization, characterization, and imaging of the GNFs used in this study can be found in Legrand et al. (2016).

Before data acquisition, the temperature of the cold plate is set to either -5, -10, or -20 °C. Once the target temperature is reached on the cold plate surface, one of the three types of droplet compositions used is deposited onto the sample plate using a Hamilton model 701RN 10 μL syringe. The three droplet types have a volume of 10 μL and composed of either (i) RO water (0.22 μm filter, conductivity of 10 μS, total organic content of less than 10 ppb), or O-GNF nanofluids

containing (ii) 20 or (iii) 100 ppm of the O-GNF dispersed in RO water. The temperatures and concentrations indicated above correspond to the same regime of experiments as Ivall et al. (2015) who used functionalized multi-walled carbon nanotubes (MWCNTs); these results will be used as a point of comparison. The sample plate consists of a 1 mm thick copper plate covered with a single layer of poly(tetrafluoroethylene) (PTFE) tape (TaegaSeal, Mil-T-277730A, 0.064-0.089 mm thick). This tape is replaced for each new run as it had been observed in initial tests that reusing the same strip affected nucleation temperatures. The droplet is deposited to have a consistent contact angle between runs. The sample plate is then transferred to the surface of the cold plate, and image capture is initiated. The formation of dendritic ice and, more commonly, the appearance of a solid front at the bottom of the droplet is used to visually detect the beginning of nucleation for the morphological experiments. The time elapsed for the droplet to freeze completely is determined through timestamps of the solidification video. The accuracy of these measurements is approximately ±0.1 s. For thermocouple experiments, used to determine nucleation temperature T_N, an Omega type K thermocouple (0.25 mm in diameter, TJ36-CASS-010G-3, calibrated to ±0.2 °C accuracy) is inserted into the droplet and placed at its base where nucleation begins. Crystal growth is an exothermic process, and thus the beginning of nucleation is marked by a sudden temperature increase. For all experiments, the velocity of the solidification front is calculated by dividing the total height of the frozen droplet by the solidification time. The total height of the droplet is also measured prior to freezing to quantify any height changes during the solidification process. After freezing is complete, the cold plate is turned off, and the system is allowed to return to room temperature. When the droplet thaws completely, an image is taken to observe nanoparticle dispersion. The droplet is then wiped off, the PTFE strip removed, and the copper

plate dried before a new PTFE strip is set, and the subsequent experiment can begin. The average room temperature and humidity were approximately 21 °C and 30%, respectively.

RESULTS AND DISCUSSION

1. EFFECT OF DRIVING FORCE ON CRYSTALLIZATION VELOCITY AND CORRELATION TO NUCLEATION TEMPERATURE

The freezing behaviour for water (no colloidal phase) and two concentrations of surface-functionalized graphene nanoflakes, each at three cold plate temperature settings, was analyzed. This was to evaluate the crystallization process and morphological behaviour of graphene nanofluids over a range of driving forces. A "driving force" is defined as the difference between the two-phase equilibrium temperature of 0 °C at atmospheric pressure and the temperature of the droplet at the time it nucleates. A higher driving force, therefore, indicates a greater supercooling of the system and, thus, colder experimental temperatures. It was assumed that the concentrations of 20 and 100 ppm were sufficiently small for the presence of O-GNFs to have a negligible impact on the thermodynamic properties of the system at equilibrium.[11, 21-23]

The sessile droplets were frozen to completion based on visual inspection. Figure 3, 4, and 5 show the nucleation events at the -5 °C cold plate setting for the three droplet compositions. Those for the -10 °C setting are found in Figure 6, Figure **7**, and Figure **8**. The morphologies at the -20 °C setting are in Figure 9, Figure **10**, and Figure **11**. In each figure, the sequence is as follows. Image (a) presents the droplet in its liquid form immediately before nucleation, along with T_N, the droplet temperature at the moment of nucleation, calculated from the correlation found in the previous section of this study. Image (b) shows the droplet shortly after nucleation. Images (c-e) illustrate the progression of the solidification of the droplet where (c) is when approximately 40%

of the height is frozen. Image (d) is for about 60%, and image (e) is for about 80% of the droplet height. Present in the upper-left corner of images (b-e) is the time elapsed since nucleation. Each experimental condition presented consists of at least five replicates to ensure the reproducibility of the observed morphological behaviour.

The solidifications at -5°C setting are characterized by a relatively leveled, planar boundary developing gradually from the base of the droplet. As can be seen in Figure 3b, 4b, and Figure **5**b, there was minimal dendritic growth. For the higher driving force experiments using -10°C and -20°C plate temperature, nucleation was easily discerned by the millisecond-scale growth of dendritic branches stemming from the droplet's base through to the liquid bulk. These can be seen in the (b) frames of each of Figures 6, 7, 8, and Figures 9, 10, 11. This could sometimes result in the appearance of an entire solid layer on the liquid/air interface, as in Figure 9b. From the thermocouple experiments (not pictured), each nucleation event, regardless of driving force or O-GNF loading, was accompanied by an exothermic release of heat where the temperature of the system rose to an equilibrium. After nucleation, the conversion of the remaining liquid bulk to solid ice was completed by a level, planar front ascending from the base of the droplet. For all experimental conditions, the end of the solidification process was marked by the formation of a pointed tip near or at the top of the droplet. This tip or cusp phenomenon is attributed to the expansion of water during the solidification phase and is well-documented in literature.[18, 24-27] Again, only the first two stages of the crystallization process are observed in this study. The solid-state adjustment stage of the process is not considered but would be expected to occur if experimental timescales were lengthened. It can be noted that the crystallization behaviour described above is exceedingly similar to that observed in previous studies using MWCNTs[23],

which indicates that these nanoparticles, regardless of size or aspect ratio, may not affect the fundamental mechanisms of crystallization.

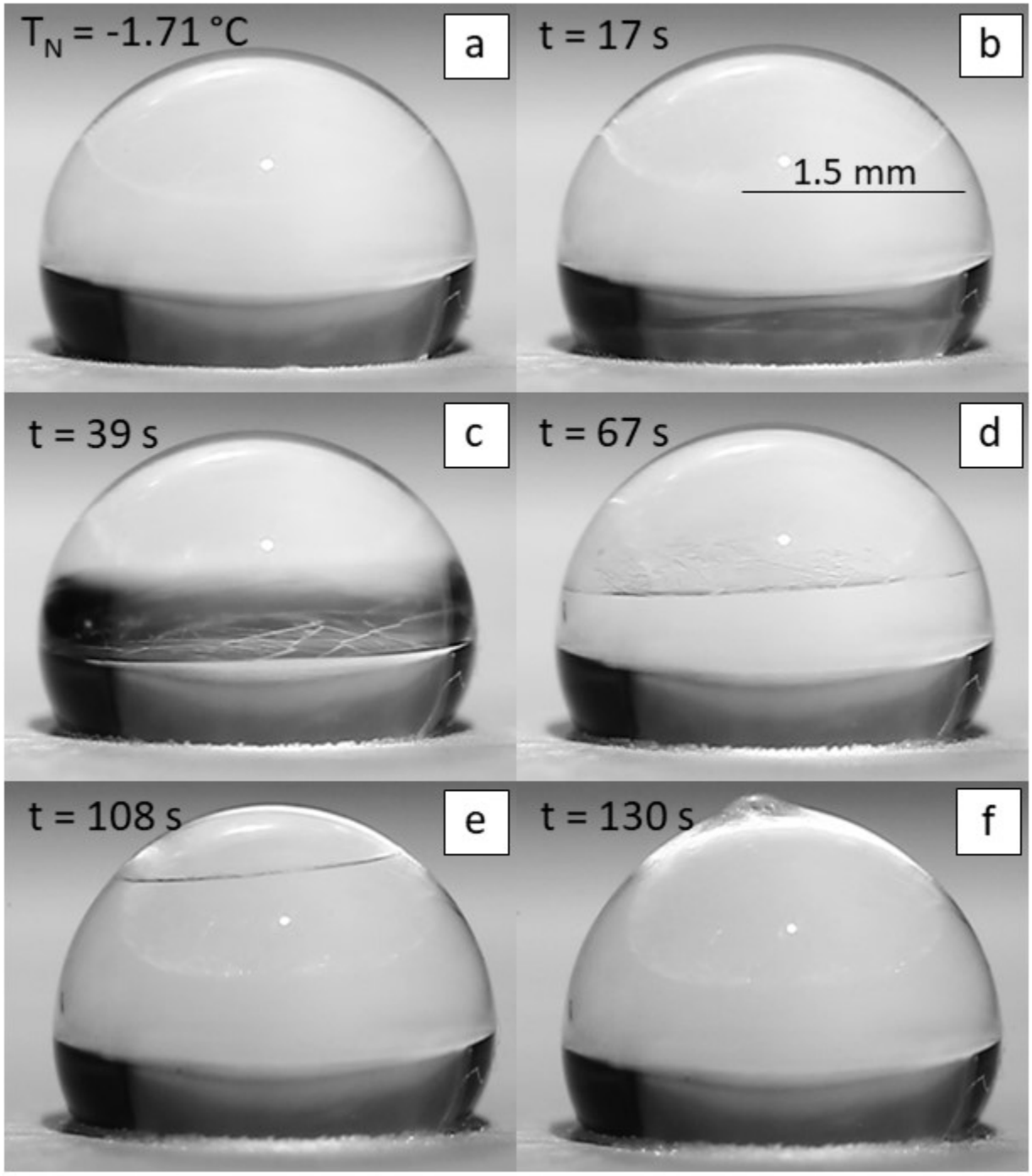

Figure 3. Pure Water Crystallization, -5°C Cold Plate Setting

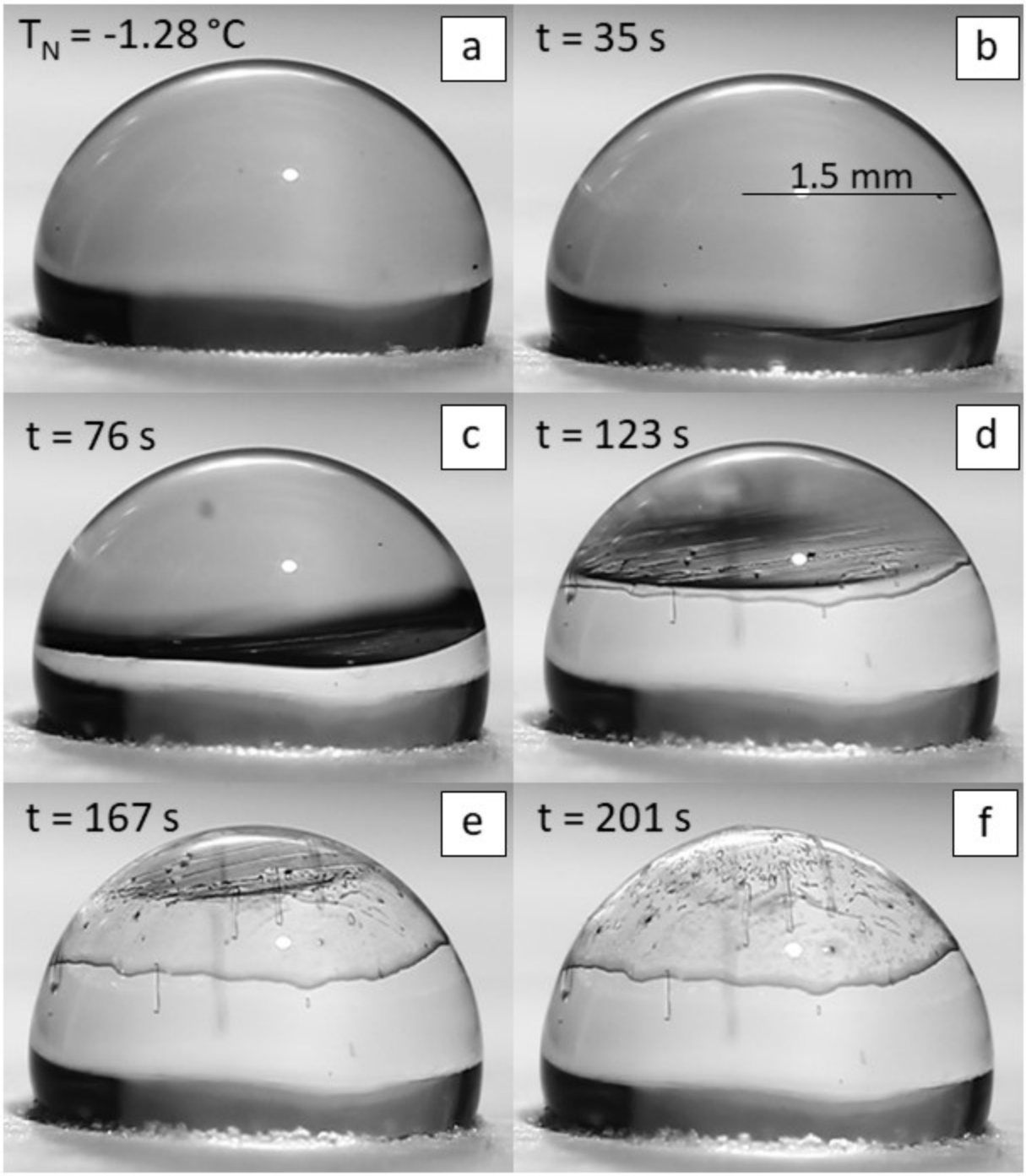

Figure 4. 20 ppm O-GNF/Water Crystallization, -5°C Cold Plate Setting

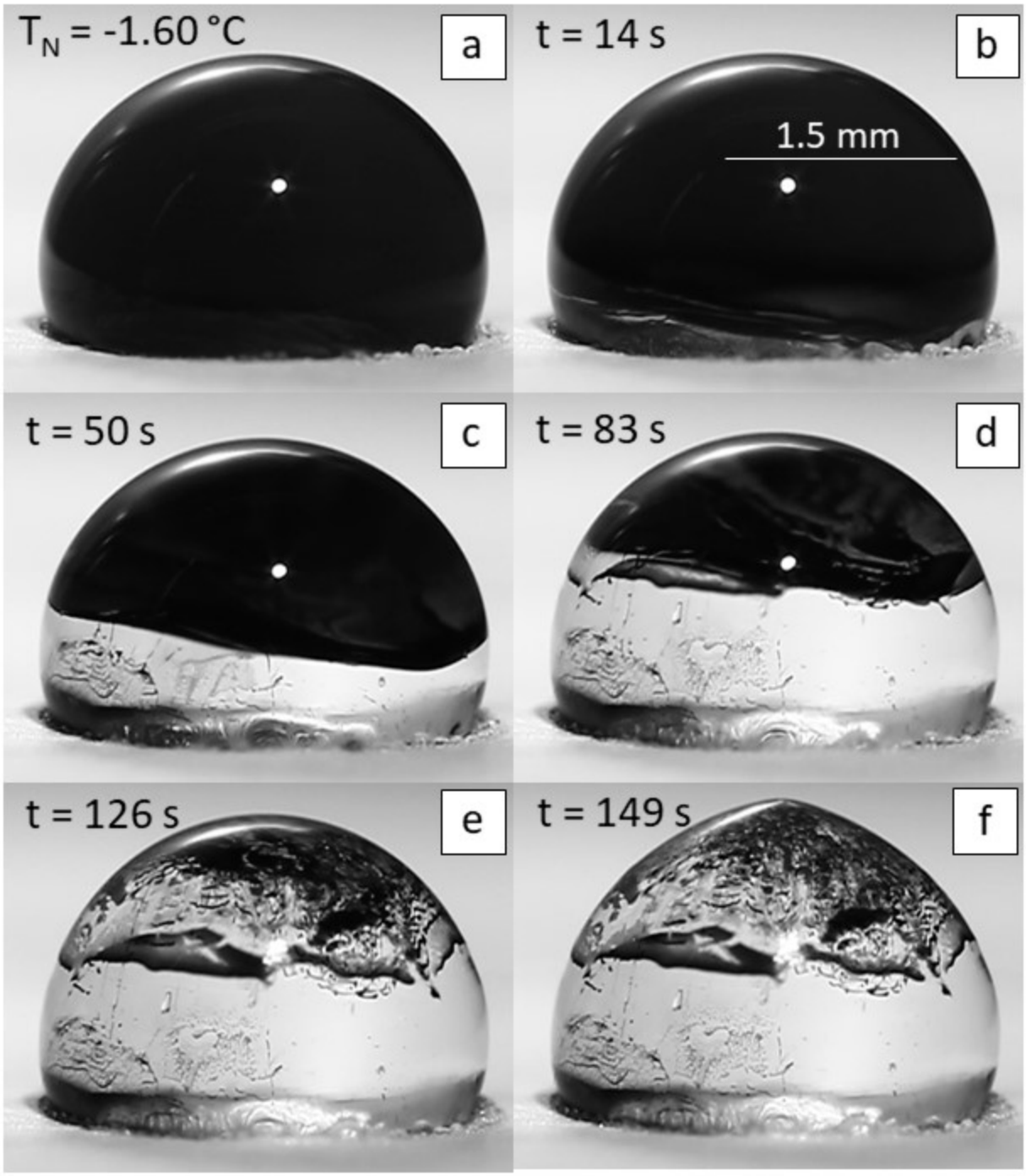

Figure 5. 100 ppm O-GNF/Water Crystallization, -5°C Cold Plate Setting

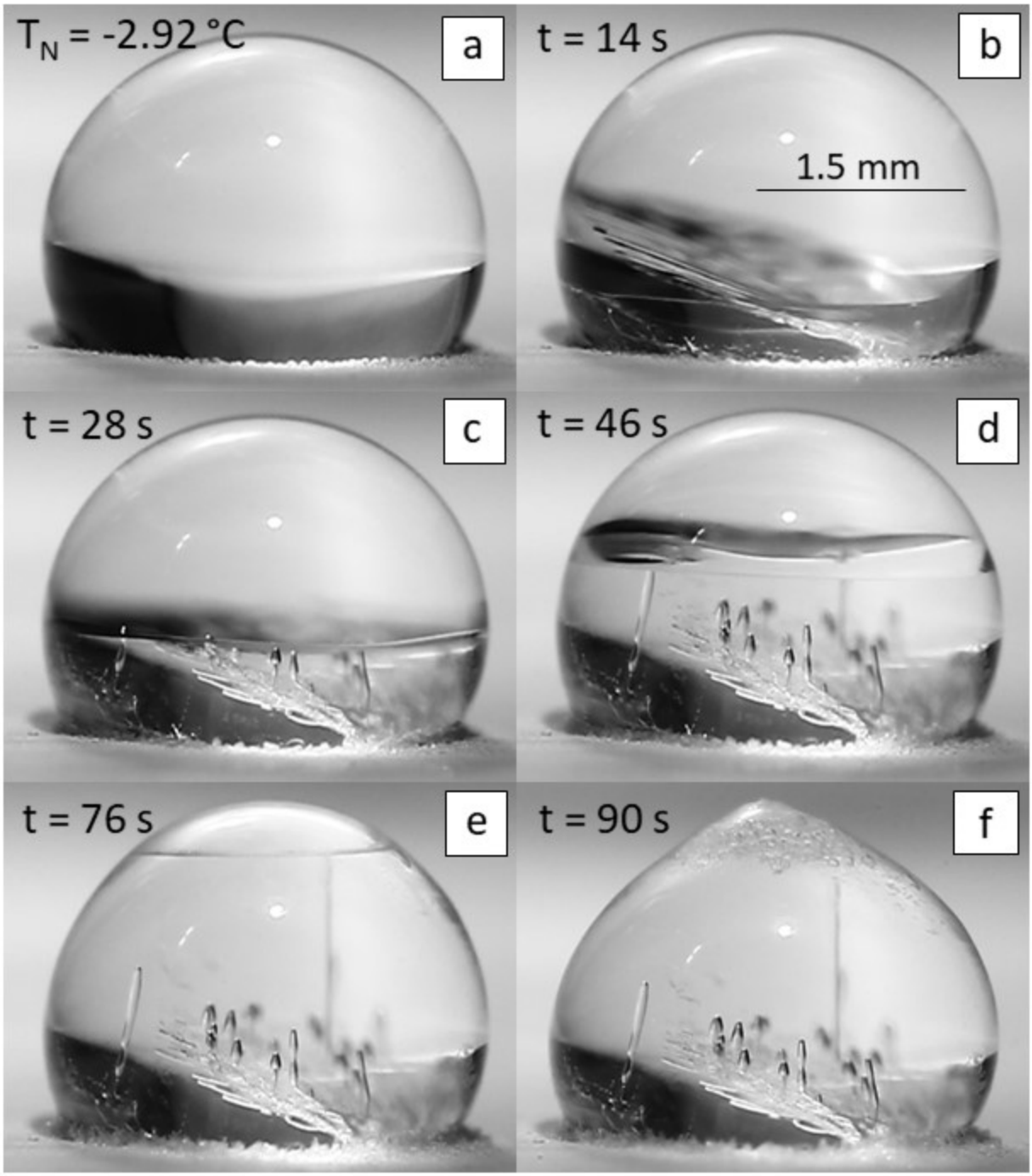

Figure 6. Pure Water Crystallization, -10°C Cold Plate Setting

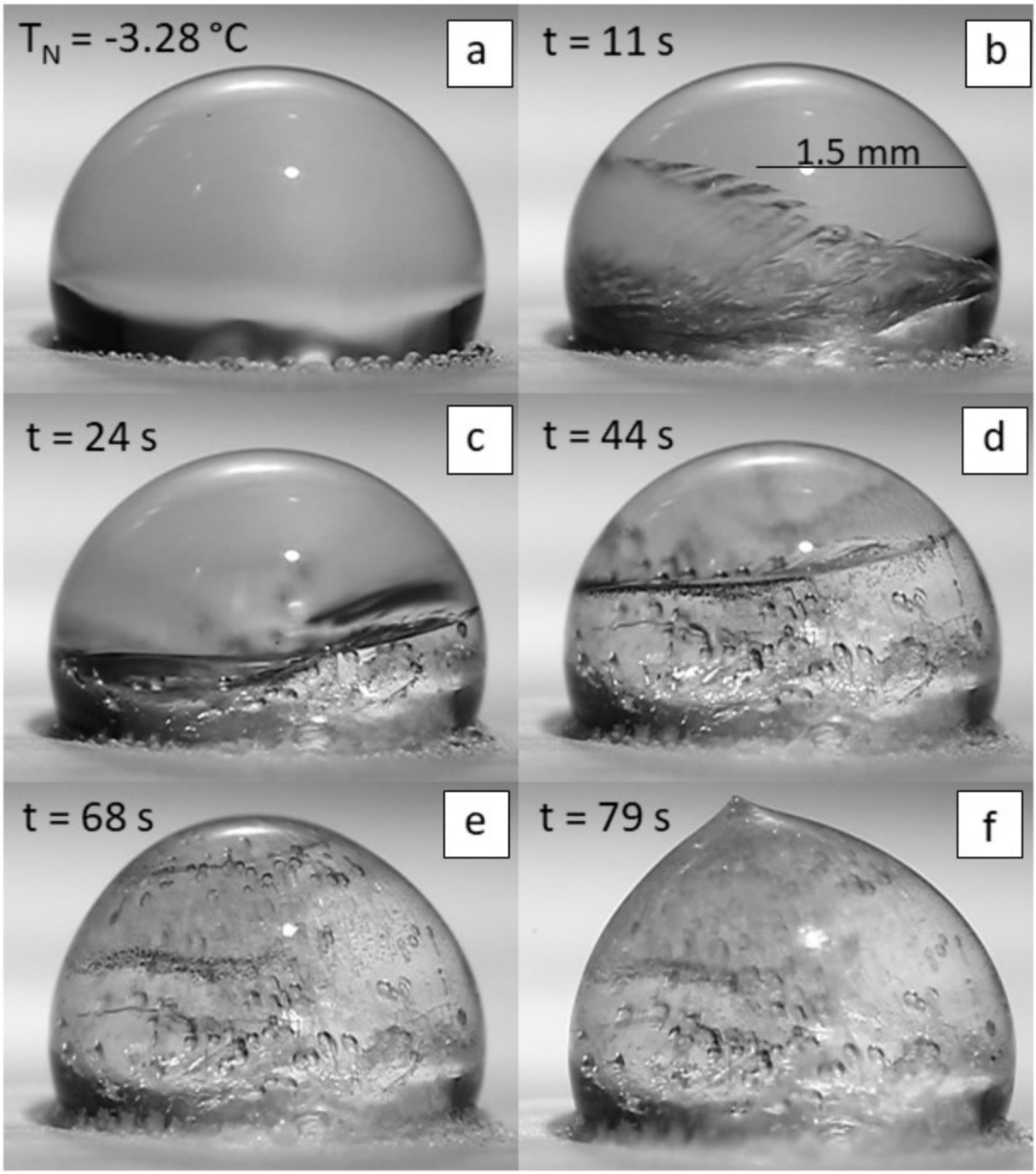

Figure 7. 20 ppm O-GNF/Water Crystallization, -10°C Cold Plate Setting

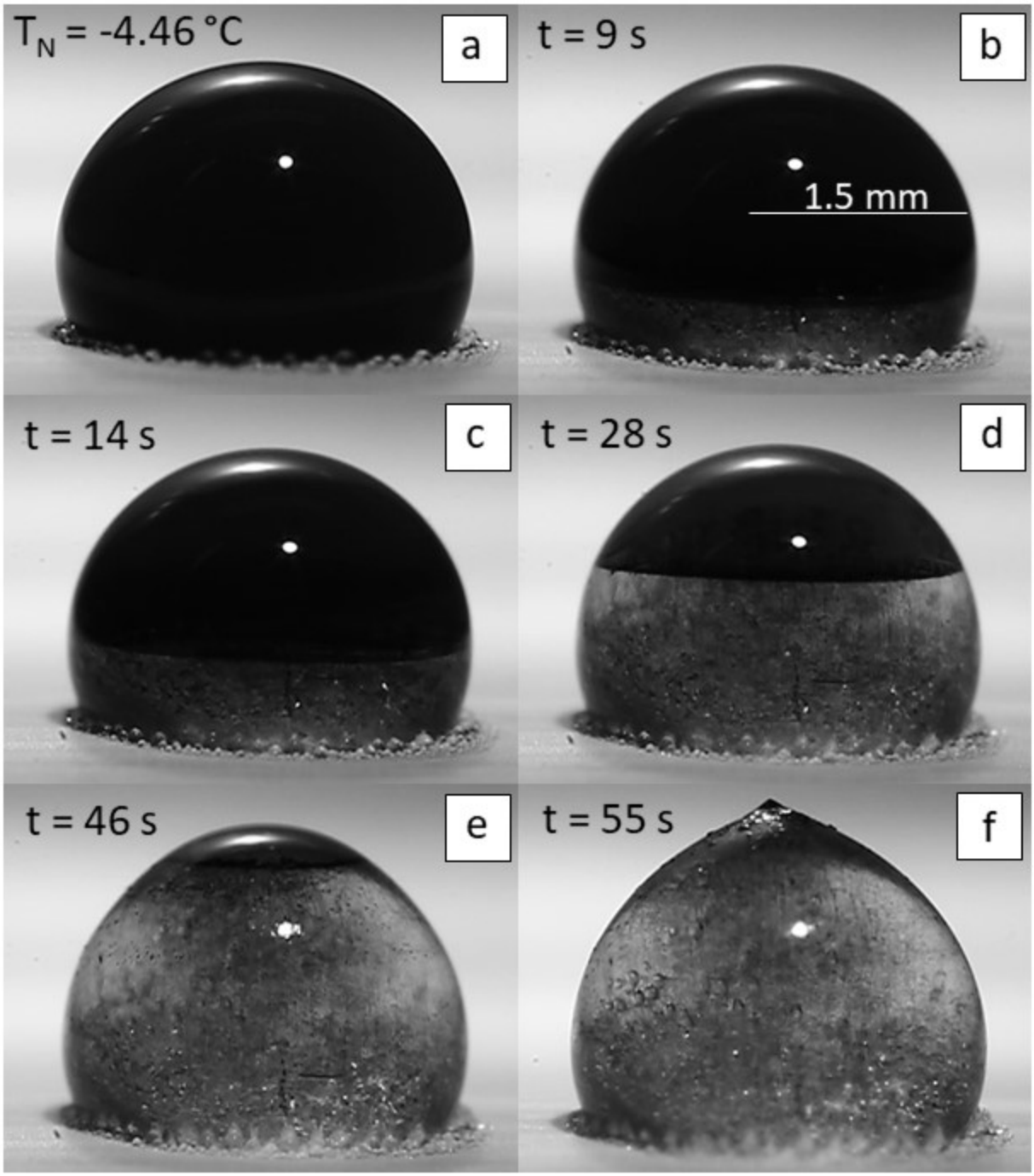

Figure 8. 100 ppm O-GNF/Water Crystallization, -10°C Cold Plate Setting

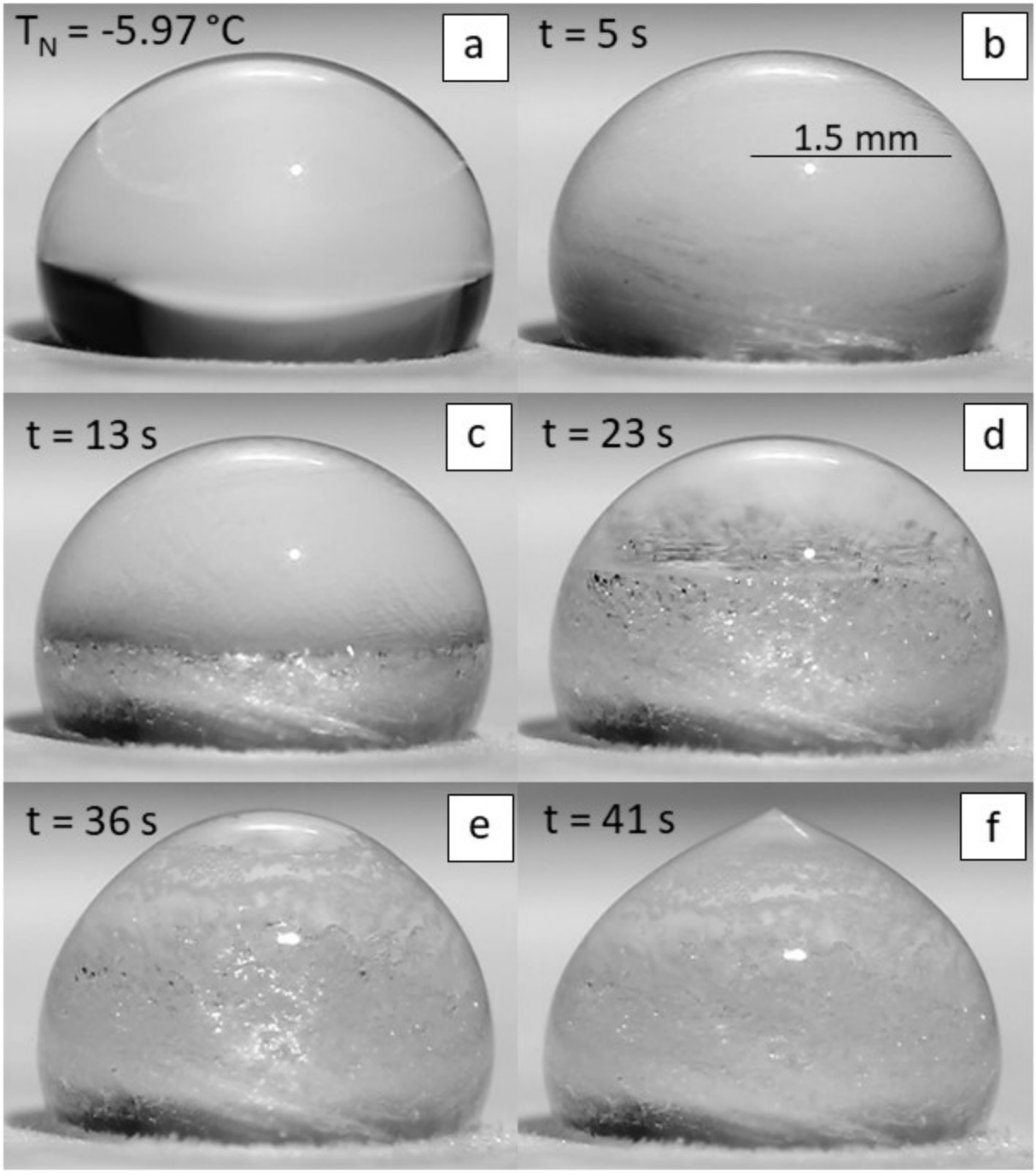

Figure 9. Pure Water Crystallization, -20°C Cold Plate Setting

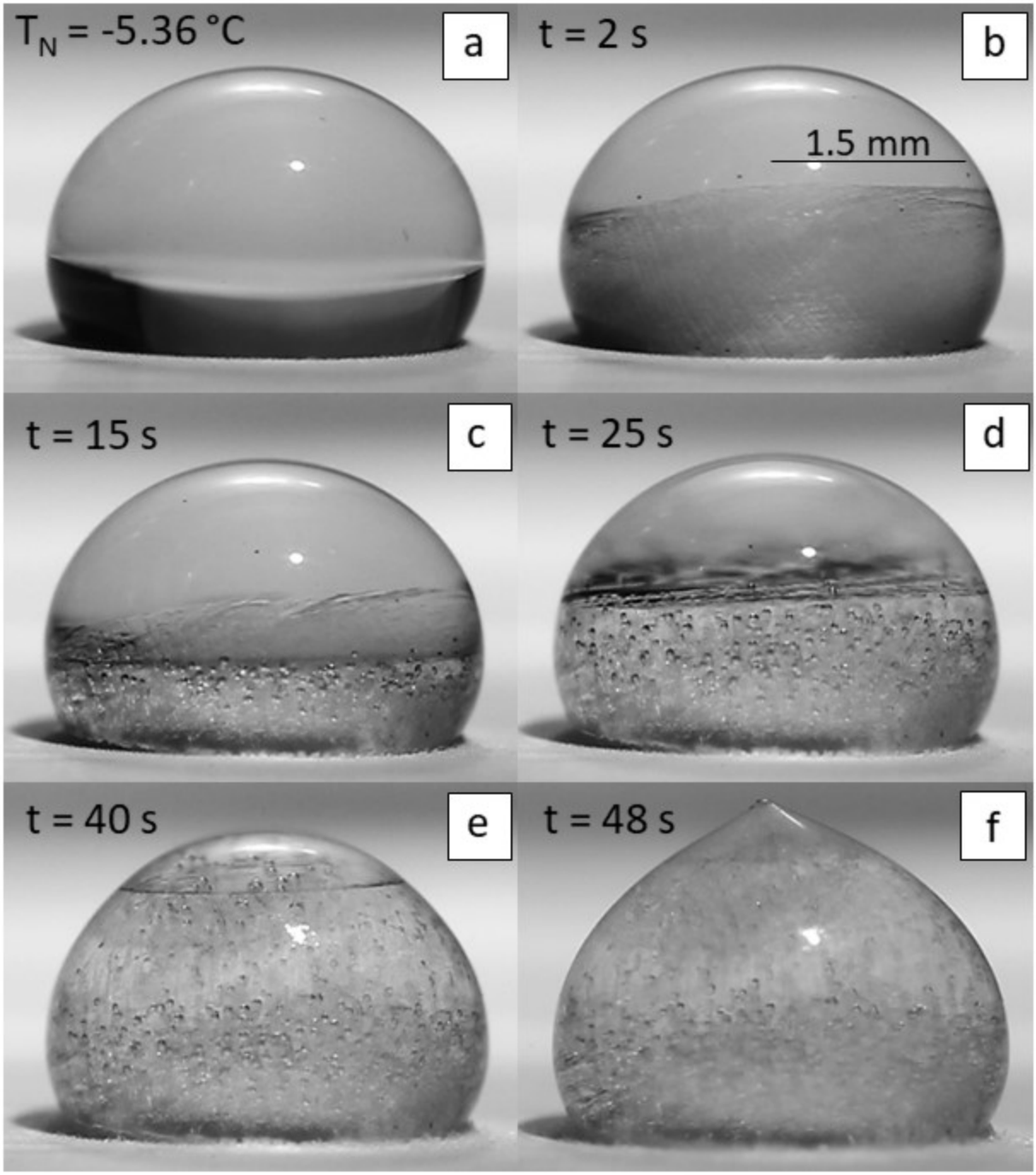

Figure 10. 20 ppm O-GNF/Water Crystallization, -20°C Cold Plate Setting

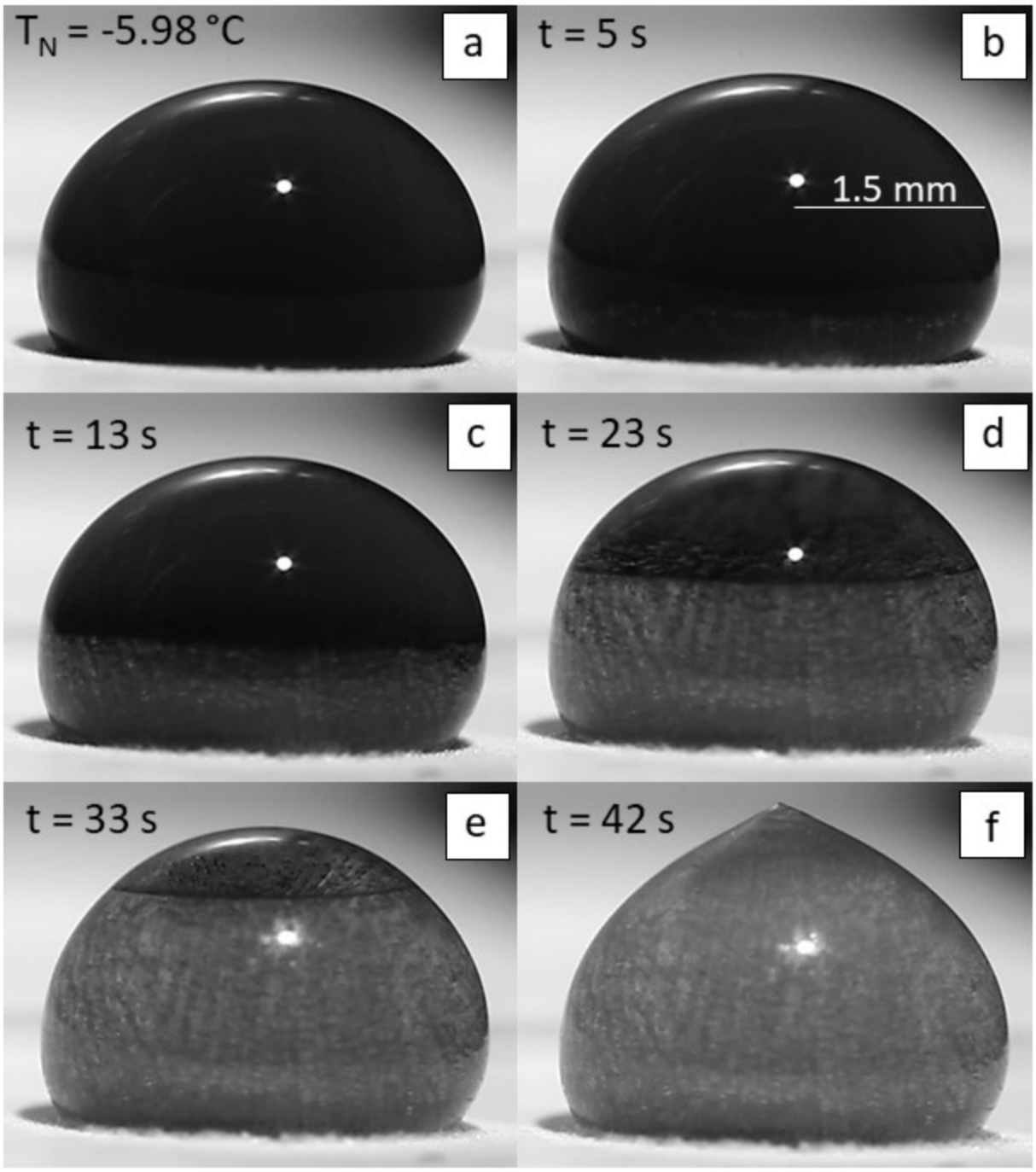

Figure 11. 100 ppm O-GNF/Water Crystallization, -20°C Cold Plate Setting

For each set of experimental conditions, the crystallization front velocity (V_F), the temperature of the droplet at nucleation (T_N), as well as the crystal morphology during the solidification process were investigated. The nucleation temperature must be measured to relate the degree of supercooling to the morphology of the system. However, the insertion of a thermocouple into the droplet during image capture will naturally affect its morphology. The supercooling/morphology analyses were therefore decoupled but reconnected through the front velocity, as there are close links between the three properties.[28-29] Experiments were thus performed to correlate front velocity and nucleation temperature (or driving force more precisely). This correlation was used to back-calculate the nucleation temperature of the morphology experiments by using the measured V_F as an input. Note that the front velocity does not take into account phase boundary acceleration or deceleration, which result from changes in height or available surface area for heat transfer[30]. Instead, this velocity can be considered an average over the height of the droplet. The dataset acquired through these experiments is presented in Figure 12. Ten replicates were performed for each cold plate temperature/concentration combination for a total of 90 data points. The trend observed in Figure 12 shows that the front velocity increases with nucleation temperature, which is consistent with other crystallization processes found in literature.[19] Essentially, heat transfer is enhanced as the departure from equilibrium becomes greater; thus, the rate of solidification is increased.[19] As no difference in behaviour was found among the three O-GNF concentrations at any given supercooling, results for all conditions are shown in the same colour in the figure. An in-depth statistical analysis determining any effect of O-GNF concentration on nucleation temperature is beyond the scope of this study. A modified Noyes and Whitney growth model has been used to describe the relationship between temperature and crystallization velocity in previous

investigations.[9, 23] For processes limited by heat transfer, velocity is expressed as an exponential function of the driving force, as shown in Equation 1.

$$V_F = A(T_{eqm} - T_N)^B = A(DF)^B \qquad \text{Equation 1}$$

Where V_F is the velocity of the solid front in μm/s, DF is the driving force or degree of supercooling in °C, A is a fitted parameter in μm/(s °C^B), and B is a dimensionless fitted parameter. The curve for the model (shown as a solid line) is shown in Figure 12, and the corresponding empirical constants are given in Table 1. Their 95% confidence intervals are also given in the table and delimited by dashed lines on either side of the trendline. Most of the experimental data lie within this region's limits. For the data set acquired, the fitted parameters were determined to have values of 8.80 μm/(s °C^B) and 1.10 for A and B, respectively. Note that these values are likely unique to this system, including the setup and lab conditions. Crystallization processes will commonly have some scatter as imperfections, grain boundaries, trapped particles, and other crystallographic factors that influence crystal growth cannot be controlled.[20] Furthermore, the spread of the data increases significantly with the driving force, and the nucleation temperatures are warmer than the temperatures of the cold plate settings. Nucleation as a phenomenon is intrinsically stochastic, though the degree of a system's departure from equilibrium is related to the probability of the occurrence of a nucleation event.[20] At lower driving forces, there is a relatively little impetus for nucleation, which gives time to the system to achieve a steady-state temperature. This temperature is warmer than the cold plate setting due to the warming effects of ambient air. At higher driving forces, there is a greater probability of nucleation, and thus, it occurs over a range of supercooling levels. This makes nucleation more likely to occur before the coldest, achievable steady-state temperature is reached.

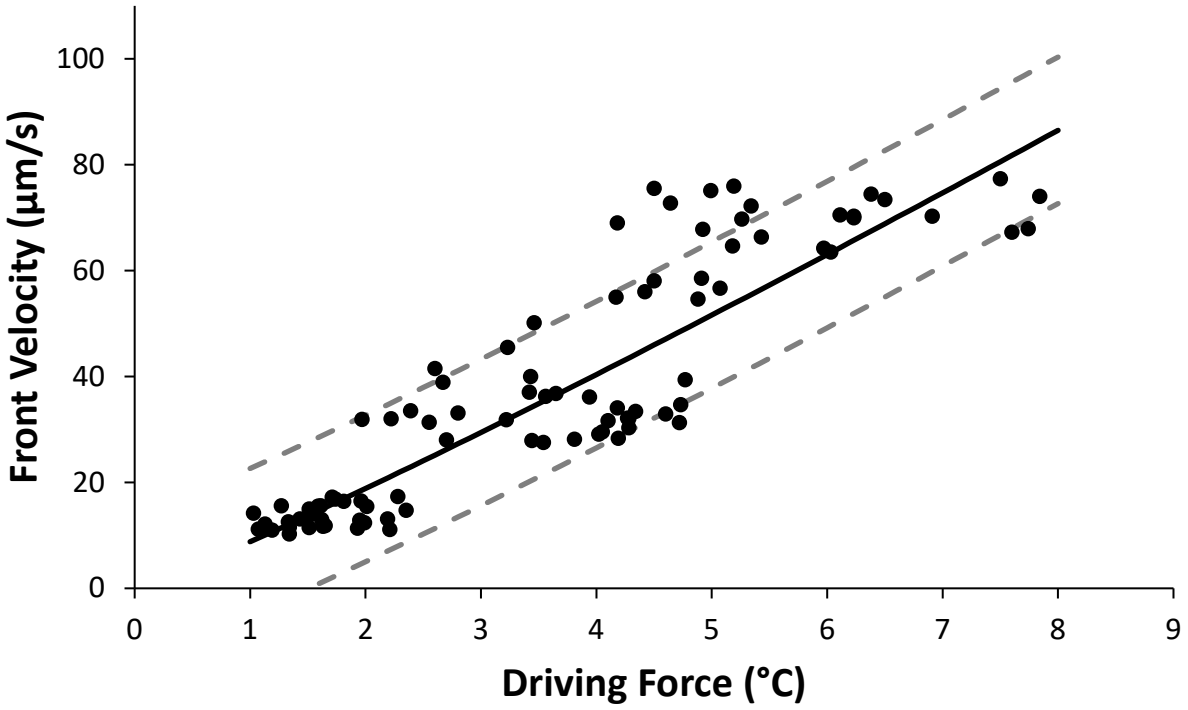

Figure 12. Correlation of Front Velocity and Nucleation Temperature with 95% Confidence Intervals

Table 1. Empirical Constants for Front Velocity as a Function of Driving Force using an Exponential Relationship with 95% Confidence Intervals

Parameter	Value	95% Confidence Interval
A [µm/(s °C^B)]	8.80	1.14
B [Dimensionless]	1.10	0.10

The nucleation temperatures (T_N) for each experimental cold plate setting/O-GNF concentration combination were calculated from the correlation and are given in Table 2. As in the correlation, the front velocity increased with the increased driving force. At the -5 °C cold plate setting, the nucleation temperatures ranged from -1.03 to -2.35 °C. For the -10 and -20 °C settings, these

ranges were -1.97 to -4.77 °C and -3.23 to -7.84 °C respectively. The solidification speeds for the thermocouple experiments were generally higher than those for the morphological experiments. Consequently, the extrapolated nucleation temperatures found for the thermocouple-free morphological experiments are warmer than the temperatures recorded when the thermocouple was present. This could be due to nucleation stochasticity, or the thermocouple itself may be acting as a surface for more energetically-favourable crystal growth.[31] Regardless, there remains a strong correlation between nucleation temperature, front velocity, and morphology, and, thus, the change in velocity/temperature would affect the droplet's morphological behaviour.

While not measured, usually, the initial nucleation event occurred more quickly at the colder cold plate settings. Though it may appear accurate for the -10 and -20 °C settings, it could not be determined if the front velocity decreased as the concentration increased due to, for instance, the O-GNF weighing down the front or inhibiting crystal growth. A more robust, in-depth study of this particular phenomenon, which is beyond this study's scope, would be required to assess any crystal growth effects of this nature.

Table 2. Nucleation Temperatures (T_N) Calculated from Crystallization Front Velocities (V_F) at Three Different Cold Plate Settings for Morphological Experiments

Plate Setting:	-5 °C		-10 °C		-20 °C	
Concentration	**V_F (µm/s)**	**T_N (°C)**	**V_F (µm/s)**	**T_N (°C)**	**V_F (µm/s)**	**T_N (°C)**
Pure Water	11.36	-1.26	42.52	-4.19	61.13	-5.83
20 ppm O-GNF	15.86	-1.71	30.92	-3.14	56.28	-5.41
100 ppm O-GNF	11.33	-1.26	27.05	-2.78	53.50	-5.17

In comparison with previous studies, it was found that the front velocities in this study were broadly similar though correlated to somewhat warmer nucleation temperatures.[23] This is likely

due to the system-specific nature of the correlation. For example, a higher humidity would result in more water particles in the air around the droplet. These particles are much smaller than the droplet and thus are more likely to nucleate quicker. There could then be a bridging effect wherein the nucleation of the smaller particles results in the nucleation of the droplet. The droplets would, therefore, nucleate in shorter time frames than expected and thus would not have sufficient time to reach lower temperatures.

2. EFFECT OF DRIVING FORCE ON GNF DISPERSION IN THE CRYSTAL PHASE

The effects of temperature on the morphology of the droplet during crystallization were assessed at cold plate settings of -5, -10, and -20 °C and O-GNF concentrations of 0, 20, and 100 ppm. Note that results (Table 2) are always in terms of cold plate setting as the driving force (or degree of supercooling) as nucleation varied between droplets.

The droplets of pure water were transparent prior to nucleation. The cloudiness observed in the figures is a result of the overhead lighting and reflective PTFE strip underneath. The dark area visible in the lower quarter of some droplets, particularly visible in image (a) of Figures 3-11, are also caused by lighting effects and should not be confused as a solid front. All droplets containing O-GNF exhibited uniform darkness prior to nucleation. The opacity of these droplets was relative to their concentration. While the presence of some small clusters is typical for any suspension, the droplets are largely homogeneous, which indicates a well-dispersed, stable nanofluid. Regardless of concentration, transparency of the droplet was significantly reduced by the formation of ice. , The ice formed from pure water at the -5 °C setting shows few imperfections and a fair clarity. On the solid/liquid interface of the droplets containing O-GNFs, such as in Figure 4 and Figure **5**, some black clumps are visible. This suggests that there is some clustering of nanoflakes along the

solid surface. From the moment of nucleation onward, the O-GNFs were continuously driven into the liquid phase by the rising solid front which was relatively leveled. This eventually resulted in some small craters of O-GNF at the top of the droplet. However, as can be seen at the midpoint of the droplets in Figure 4f and Figure **5**f, some O-GNF was expelled to the sides of the frozen droplet rather than the top. The latter O-GNFs escaped the droplet during brief decelerations in the upward movement of the solid front and flowed towards the sides before the front continued to move. This is a somewhat different behaviour compared to that observed by Ivall et al. (2015) under the same conditions but with MWCNTs. In that study, nearly all of the nanoparticles were found in a single large crater at the top of the droplet after freezing was complete, and no MWCNTs escaped the solution at other times.[23] It is possible that, due to their string-like structure, the MWCNTs become physically entangled as they cluster and thus move as a single, solid mass when pushed by the front.[23] The more square prism-like O-GNFs may be able to slip off each other and would thus not become entangled. While nanoflakes have higher surface energies than nanotubes, the hydrophilic groups on their surfaces would repel each other and allow the slip to occur.[32] These combined effects would permit them to flow more freely during the deceleration of the front. In other words, the shorter geometry of the O-GNFs compared to the very long MWCNTs may result in greater particle mobility when a system slowly undergoes a phase change from liquid to solid. Nonetheless, in both cases, at low crystallization speeds, and thus low driving forces, the nanoparticles are completely expelled from the final crystal structure, and the ice (of remarkable clarity) underneath the particles is virtually free of either O-GNF or MWCNT.[23] It is likely, therefore, that neither particle was sufficiently undercooled for heterogeneous nucleation to occur on their surface (i.e. no ice grew from the nanoparticles themselves) and thus they were pushed out of solution by the solid phase which emanated from the base of the droplet.[31]

At the -10 °C setting, there is a significant change in the morphology of the freezing nanofluid. In Figure 6b and Figure **7**b, there is evidence of more distinguishable dendritic offshoots formed at nucleation, which consisted largely of horizontal, curved branches. Dendrite formation was followed by the slower ascension of the solid front. It was also found that air bubbles became trapped within the crystal structure, which created pockets. These elliptical bubbles were relatively dispersed through most of the droplet, though appeared to have a somewhat greater concentration (in terms of number, not necessarily volume) near the top. This effect is clearest in Figure 6f. The solubility of air in ice is three orders of magnitude smaller than in liquid water.[33] Thus, there is a tendency for bubbles to form during the liquid to solid phase change of water. In the case presented in Figure 6f, Figure **7**f, and Figure **8**f, the base of the droplet contains a zone with a significant number of bubbles, which is followed by a zone of clearer ice before air bubbles reappear near the top. In sessile droplets and other static systems, the extent and morphology of trapped bubbles such as these are largely determined by the speed of crystallization.[28] The local concentration of air in the liquid at the moving front is increased as it is rejected by the solid phase. Air molecules can then create pockets by nucleating into a separate phase if supersaturation is reached.[28] Nucleated air bubbles can diffuse away from the interface and into the liquid bulk if the growth rates of the crystal are sufficiently slow. This is the case at low degrees of supercooling such as at the -5 °C setting. At higher driving forces, crystallization velocities are increased to the extent that this diffusion is overcome, and the air becomes entrapped. Therefore, the zoning pattern found in the higher driving force droplets may arise from the particular growth rate to air precipitation ratio of each droplet.[28] Another significant morphological difference at higher driving forces is the inclusion of O-GNFs within the solid droplet. There is some degree of encapsulation of clusters of O-GNF in the ice visible in Figure 7 and Figure **8**. However, they are not present within the ice

matrix itself. Instead, they are trapped within the volume of the air bubbles present, such as in Figure 7e. This is further evidence that heterogeneous nucleation was not occurring on the particle surface and that individual particle dispersion within the solid at these solidification speeds was not attained. There is also evidence that the speed of crystallization was not constant throughout the phase change process as the O-GNF clusters appear to be localized to the air bubbles specifically. There is higher heat transfer at the upper and lower portions of the droplet. They therefore freeze more quickly and contain more air bubbles and O-GNFs than the middle section of the droplet where the front decelerates. As mentioned, this interfacial deceleration allows the O-GNFs and the air bubbles to migrate further into the liquid bulk. It follows therefore that there is still some O-GNF expelled from the droplet near the center (see Figure 7e) but to a significantly lesser extent than at the low driving force. Generally, particle rejection became less severe as the driving force increased. This behaviour at the -10 °C setting matches much more closely with the phenomena observed by Ivall et al. (2015) which may indicate that at higher driving forces, crystallization speeds become higher and potentially limit the improved mobility of the O-GNF in the liquid.

At the -20 °C setting, the formation of dendrites was at its most significant, as were the entrapment of bubbles and O-GNF inclusion. The dendrites extended significantly further, sometimes appearing over the entirety of the droplet, such as in Figure 9b. They also had a more vertical orientation than those at lower driving forces, which is visible in Figure 9b, Figure **10**b, and Figure **11**b. While difficult to see, they also have finer, more sharp branching.[34] The entrapped bubbles appeared more evenly distributed throughout the droplets and were generally smaller in size. Furthermore, most if not all of the O-GNF was confined to the solid droplet when the phase change had completed. The O-GNFs were found in localized, clumped masses, which followed

the bubble and dendrite patterning. This is similar to what occurred at the -10 °C setting. It should be noted that the O-GNFs are stably dispersed in the liquid and do not, like the air dissolved in the liquid phase, nucleate into a distinct phase due to supersaturation. In fact, their exclusion from the water phase is what leads to their grouping together. However, despite their uniform distribution, the formation of O-GNF clusters suggests that nanoparticle dispersion within the solid crystal is not attained in the bulk at high crystallization velocities. For instance, in Figure 11 the dispersion is very good, but this is still a dispersion at the grain boundaries of a very fine dendritic structure and not dispersion in the bulk of the single crystal phase. The behaviour at the -20 °C setting was once again similar to that of Ivall et al. (2015), with no significant differences in morphology found. Furthermore, for all driving forces and concentrations in both studies, the presence of nanoparticles was not found to have an effect on the morphology of the freezing droplets as they were not included in the phase change process itself. However, the faster solidification and finer dendritic structure allowed much more overall dispersion of the nanomaterial throughout the system. This may strongly affect important physical properties of the solid droplet. These would include the mechanical properties of the nanocomposite as well as thermal and electrical transport properties.

The exclusion of colloidal particles from a solidifying host material is inversely related to the degree of supercooling.[23, 35] The solubility of dissolved or colloidal particles in ice is low. In terms of thermodynamics, lattice homogeneity will be exclusively favoured by the crystal system.[36] At lower degrees of supercooling, and thus low driving forces and growth rates, the crystal preferentially develops into a homogeneous array. At higher driving forces, there is a greater propensity to crystallize fully and, thus, the homogeneity of the solid matrix is reduced. Over extended periods the crystal matrix will undergo solid-state adjustments to correct irregularities

and remove O-GNFs as it is always energetically favourable to exclude impurities from the system.[20]

A critical velocity occurs at a speed for which particles, such as O-GNF, are entrapped within the crystal matrix and maintain their dispersion. It has previously been reported that this velocity is inversely proportional to the size of the entrapped particle.[35, 37-38] However, the multitude of parameters that may influence the inclusion of particles make categorizing this behaviour much more complicated. The entrapment process is usually modelled as a balance between drag forces, which push the particles towards the solid front, and repulsive Lifshitz-van der Waals forces, which push the particles into the liquid bulk.[39-41] Typical assumptions in these models include spherical particle shapes of 10 to 50 μm in diameter. Thus no Brownian or buoyancy effects are present in these systems.[39] Recently, however, more advanced models for non-spherical particles, which have greater drag forces, have been developed.[40] O-GNFs likely have increased drag forces from their square prism shape, and from the concave structure of the interface, and thus are disposed to incorporation within the solid. However they also have Brownian dispersion from their hydrophilic surface groups and are at sizes orders of magnitude smaller than in previous studies.[4] This means such nanoparticles would tend to be retained in the liquid phase. It appeared that the O-GNFs were preferentially confined to inter-dendritic spaces and air pockets (see Figure 7). Within the solid matrix, they exhibited very little particle dispersion under the given temperature conditions. This suggests that Brownian effects dominate the inclusion mechanism. At the coldest conditions, which contained finer dendrites and smaller bubbles, smaller masses of O-GNFs were seen. However, there was still no evidence of individual particle dispersion within the ice matrix. This was also the case in Ivall et al. (2015) who suggested that more severe driving forces could perhaps result in reaching a critical crystallization velocity and thus achieve some level of

dispersion.[15, 23] Crystallization velocities obtained in this study ranged from about 7 to 65 μm/s which are significantly below the critical values observed for systems with larger particles.[39] Previous studies using graphene have found critical velocities of 39 μm/s.[42] However, this number is only applicable for smaller, spherical particles that could more easily be incorporated into the solid matrix. Therefore, the critical velocity for O-GNFs was likely not reached in this study though some nanoflake effects may be obscured by other effects such as the the effect of the presence of air bubbles in the liquid on crystallization kinetics.

The driving force was also observed to affect the change in the droplet's height upon solidification. The vertical expansion, or relative change in height after phase change, of the droplet was calculated for each condition and is found in Table 3. The most significant increases in height were observed at the -10 and -20 °C settings, which is likely due to the presence of air bubbles in these systems. At the -5 °C setting, the relative height change decreased as the loading of O-GNFs increased. It is possible that the vertical expansion of the droplet was reduced by the blanket of nanoflakes present along the solid/liquid interface. This could have promoted a horizontally-favoured growth, which would lead to wider droplets. Changes in the width of the droplets were not measured, but it should be noted that the volume can be significantly impacted even by minor lateral enlargements. Furthermore, crystallization speeds are at their lowest at this driving force, which allows agglomerates to settle at the interface. This is most visible in Figure 4d and would likely have kinetic effects on crystallization. It is possible that this thickening nanoparticle layer impedes the supply of water molecules to the solid front. It could also perturb the temperature gradient in the droplet by affecting the heat transfer fields at the interface.[43] It may also be possible that the weight of the particles themselves on the front hinders growth. It follows that, as the heights were reduced artificially, the crystallization velocities were reduced as well,

and the nucleation temperatures calculated from the correlation were warmer than in reality. This is further evidence that driving forces strongly affect the morphology of nanofluids during liquid to solid phase change.

To elucidate differences between the height changes found in Table 3, Welch's t-test was performed for equal sample sizes with unequal variance. In our test, the hypothesis that the means were statistically different was rejected if t had a value greater than 0.05. Regardless of concentration, there was no statistical difference in vertical expansion between the -10 and -20 °C settings. Moving from center to rightmost column in Table 3, t values were 0.57, 0.38, and 0.83 at 0, 20, and 100 ppm respectively. These droplets have a defined volume and are limited in terms of shape by their surface tension. They, therefore, have a maximum achievable change in height while they maintain their shape. It is possible that this change is reached, or nearly reached, at the -10 °C setting and therefore are only maintained when the driving force is increased. Moreover, the bubbles and particle entrapment which occur at higher crystallization velocities could result in less resistance to the front and the reduction of the slowing effects observed at lower driving forces. Furthermore, for the middle and higher driving forces, loading did not affect the change in height. In other words, the maximum height change observed for pure water was also achieved at both 20 and 100 ppm. Indeed, at the -10 and -20 °C settings, there was no statistically significant change in vertical expansion as concentration increased. Moving down the two rightmost columns in Table 3, t values were 0.14 and 0.67 with increasing concentration at the -10 °C setting and 0.13 and 0.12 at the -20 °C setting. This behaviour at the -20 °C setting is similar to what was reported in previous studies, but the behaviour at the -10 °C setting is not. Ivall et al. (2015) found that there were reduced height changes with loading at the -10 °C setting. It is possible that the ability of the O-GNFs to slip, which could allow them greater mobility at the interface, resulted in less physical

resistance to the moving front compared to the entangled MWCNTs. This, in combination with previously mentioned effects, may, therefore, have resulted in minimal loading effects on height change at the middle setting compared to the previous study.

Table 3. Relative Percent Change in Droplet Height After Freezing

Concentration	**-5 °C Setting**	**-10 °C Setting**	**-20 °C Setting**
Pure Water	11.7	20.0	20.8
20 ppm O-GNF	8.5	16.1	18.8
100 ppm O-GNF	4.4	17.7	16.9

3. MELTING OF FROZEN NANOFLUID DROPLETS

The frozen droplets were melted at room temperature for five minutes, and the visual characteristics of the resultant nanofluid were examined to assess O-GNF stability when returning from a liquid to solid conversion. Figure 13 shows the behaviour of droplets thawed from all three cold plate settings for the 100 ppm O-GNF concentration. Note that the visual characteristics of melting for the 20 ppm droplets were the same as for the 100 ppm droplets. However, they were more decipherable for the latter concentration and thus only 100 ppm results are presented in this study. It was observed at both experimental concentrations that there was a significant loss of dispersion resulting from the solidification process. Before freezing, the 100 ppm droplets such as in Figure 11a appeared to have a homogeneous dark appearance. In contrast after melting one sees a transparent fluid with numerous clusters scattered throughout. The degree of supercooling likely determined the size of these clusters. At the -5 °C setting, the lowest supercooling, yields were characterized by large clusters of O-GNF having tens to sometimes hundreds of micrometres in length. These were likely a result of the formation of small craters at the top of the droplet. At the

-10 °C setting, many clusters were in the tens of micrometres range though some larger clusters were observed. This was likely the result of more particles trapped locally in the solid matrix. At the -20 °C setting, the highest supercooling, only the smallest clusters remained, though the nanofluid should not be considered dispersed. This may have resulted from nearly all of the O-GNF being trapped in smaller, local pockets. Compared to previous studies using MWCNTs, the melted droplets have a noticeably greater dispersion.[23] This may once again have been the result of MWCNT entanglement, which created much larger bundles that likely could not disentangle to a significant extent while the solid matrix deformed. There was still evidence of many O-GNF agglomerates, but the lack of entanglement may have resulted in an improved dispersion.

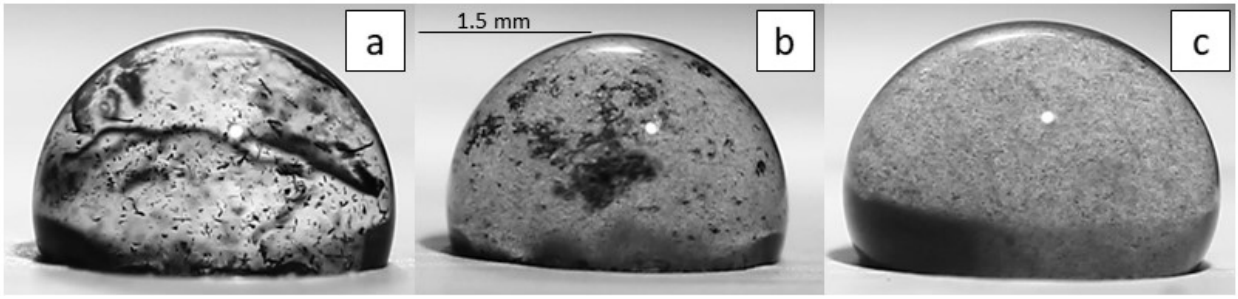

Figure 13. Droplets Containing 100 ppm O-GNF Frozen at -5 °C (a), -10 °C (b), -20 °C (c) then Melted Over 5 Minutes

In larger, closed systems (data not shown), the clusters would eventually settle to the bottom of their container. This indicated that the gravity effects of the larger O-GNF clusters overcame the Brownian agitation, which led to sedimentation.[3] However, ultrasonication was used in an attempt to recover individual suspension and break up the clusters. After 20 minutes of sonication, it was found that these clusters were mostly separated, and the dispersion had, visually, recovered some of its homogeneity. The question remains as to why, upon melting, the O-GNFs do not immediately become redispersed. As water becomes incorporated into the solid phase, the mass

fraction of nanoflakes in the aqueous phase increases. This is similar to a drying process. The increased concentration results in an increased probability of collision, particularly at the solid/liquid interface, which could result in physical contact between the particles. When water expands during phase change, the pressure within the ice matrix increases.[44] This, in combination with higher proximity, could push the repulsive potentials between the O-GNFs into a more attractive regime.[45-46] Moreover, there is an electrostatic double layer between the particles, which requires a liquid solution into which the charged ions may dissolve.[45] The concentration and distribution of charges in both the solid and liquid phase may thus be altered through the removal of the base fluid (and the creation of the solid matrix) such that interparticle repulsion is no longer favourable.[23] This would result in the presence of van der Waals attractive forces and lead to colloidal destabilization. Furthermore, at such small distances, these interactions are at an energetic minimum and thus, the particles do not separate spontaneously.[47] The loss of O-GNF nanofluid stability raises some concerns regarding the operation of nanofluid technologies since it is usually desired to maintain a maximal individual dispersion to retain the nanofluid's favourable properties. There are varying magnitudes of particle dispersion within the solid and liquid phases since these are a function of the degree of supercooling. This would lead to inconsistent system properties during the different phases of crystallization. Exposure to freezing conditions would, therefore, have to be avoided, particularly during cooling, storage, and transport applications, or the integrity of the nanofluid may be compromised. Only a single freezing event was examined in this study; a multi-cycle analysis would be vital in establishing the benefits of long term use of O-GNF nanofluid technologies.

CONCLUSIONS

The solid to liquid phase change behaviour of small, sessile water droplets was evaluated for two concentrations of plasma-functionalized graphene nanoflakes at three driving force temperatures. The degree of supercooling had the single most substantial effect on the dispersion of O-GNFs within the solid matrix for both concentrations. Low driving forces resulted in slow rates of crystallization, and thus, the O-GNFs were wholly expelled from the solid droplet, some to the sides at locations where the front slowed, but most to the top of the solid, forming craters. At higher driving forces, the O-GNFs became trapped within the solid droplet, though no individual particle dispersion was achieved in the bulk. Instead, the nanoflakes were embedded in sites of crystal imperfections such as air bubbles and inter-dendritic spaces. Still, entrapped O-GNF clusters were well dispersed in the very fine inter-dendritic regions which formed at the highest solidification rates. O-GNF clusters that formed during freezing did not disperse spontaneously upon melting. This indicated that crystallization destabilized the nanoparticles as drying-like effects may have altered the attraction properties of their surfaces. Compared to previous studies using MWCNTs, the O-GNFs were found to have higher liquid mobility at the solid front, provide less resistance to that front as it ascended, and be better dispersed after melting, which may have been because nanoflake geometry does not result in any physical particle entanglement. However, the success of nanofluid technologies is contingent on consistent, individual dispersion in the base medium. Thus, the results found here bring up significant considerations when evaluating their use in emerging transport, storage, and cooling applications.

AUTHOR INFORMATION

Corresponding Author

*phillip.servio@mcgill.ca

Author Contributions

The manuscript was written through the contributions of all authors. All authors have approved the final version of the manuscript.

ACKNOWLEDGEMENTS

The authors would like to acknowledge the financial support from the Natural Sciences and Engineering Research Council of Canada (NSERC). We would also like to acknowledge Pierre-Alexandre Pascone for the synthesis of O-GNF particles.

REFERENCES

1. Choi, S. U.; Eastman, J. A. *Enhancing thermal conductivity of fluids with nanoparticles*; Argonne National Lab., IL (United States): 1995.

2. Yu, W.; Xie, H. J. J. o. n., A review on nanofluids: preparation, stability mechanisms, and applications. **2012,** *2012*, 1.

3. Taylor, R.; Coulombe, S.; Otanicar, T.; Phelan, P.; Gunawan, A.; Lv, W.; Rosengarten, G.; Prasher, R.; Tyagi, H. J. J. o. A. P., Small particles, big impacts: a review of the diverse applications of nanofluids. **2013,** *113* (1), 1.

4. Legrand, U.; Gonzalez, N.-Y. M.; Pascone, P.; Meunier, J.-L.; Berk, D. J. C., Synthesis and in-situ oxygen functionalization of deposited graphene nanoflakes for nanofluid generation. **2016,** *102*, 216-223.

5. Shao, Y.; Wang, J.; Wu, H.; Liu, J.; Aksay, I. A.; Lin, Y., Graphene Based Electrochemical Sensors and Biosensors: A Review. *Electroanalysis* **2010,** *22* (10), 1027-1036.

6. Choi, W.; Lahiri, I.; Seelaboyina, R.; Kang, Y. S., Synthesis of Graphene and Its Applications: A Review. *Critical Reviews in Solid State and Materials Sciences* **2010,** *35* (1), 52-71.

7. Missana, T.; Adell, A., On the Applicability of DLVO Theory to the Prediction of Clay Colloids Stability. *Journal of Colloid and Interface Science* **2000,** *230* (1), 150-156.

8. Pasieka, J.; Coulombe, S.; Servio, P. J. C. E. S., Investigating the effects of hydrophobic and hydrophilic multi-wall carbon nanotubes on methane hydrate growth kinetics. **2013,** *104*, 998-1002.

9. Pasieka, J.; Hordy, N.; Coulombe, S.; Servio, P. J. C. G.; Design, Measuring the effect of multi-wall carbon nanotubes on tetrahydrofuran–water hydrate front velocities using thermal imaging. **2013,** *13* (9), 4017-4024.

10. Kumaresan, V.; Chandrasekaran, P.; Nanda, M.; Maini, A.; Velraj, R. J. I. J. o. R., Role of PCM based nanofluids for energy efficient cool thermal storage system. **2013,** *36* (6), 1641-1647.

11. Chandrasekaran, P.; Cheralathan, M.; Kumaresan, V.; Velraj, R. J. I. J. o. R., Solidification behavior of water based nanofluid phase change material with a nucleating agent for cool thermal storage system. **2014,** *41*, 157-163.

12. Wang, J.; Xie, H.; Xin, Z. J. J. o. a. p., Thermal properties of heat storage composites containing multiwalled carbon nanotubes. **2008,** *104* (11), 113537.

13. Mo, S. P.; Chen, Y.; Yang, J. Y.; Luo, X. L. In *Experimental study on solidification behavior of carbon nanotube nanofluid*, Advanced Materials Research, Trans Tech Publ: 2011; pp 333-336.

14. Kumaresan, V.; Velraj, R.; Das, S. K. J. H.; Transfer, M., The effect of carbon nanotubes in enhancing the thermal transport properties of PCM during solidification. **2012,** *48* (8), 1345-1355.

15. McElligott, A.; Uddin, H.; Meunier, J.-L.; Servio, P. J. E.; Fuels, Effects of Hydrophobic and Hydrophilic Graphene Nanoflakes on Methane Hydrate Kinetics. **2019,** *33* (11), 11705-11711.

16. Glicksman, M. E., 16 - Dendritic Growth. In *Handbook of Crystal Growth (Second Edition)*, Nishinaga, T., Ed. Elsevier: Boston, 2015; pp 669-722.

17. Feuillebois, F.; Lasek, A.; Creismeas, P.; Pigeonneau, F.; Szaniawski, A., Freezing of a Subcooled Liquid Droplet. *Journal of Colloid and Interface Science* **1995,** *169* (1), 90-102.

18. Tavakoli, F.; Davis, S. H.; Kavehpour, H. P., Freezing of supercooled water drops on cold solid substrates: initiation and mechanism. *Journal of Coatings Technology and Research* **2015,** *12* (5), 869-875.

19. Pruppacher, H. R., Interpretation of Experimentally Determined Growth Rates of Ice Crystals in Supercooled Water. *The Journal of Chemical Physics* **1967,** *47* (5), 1807-1813.

20. Mullin, J. W., *Crystallization*. Elsevier: 2001.

21. Sathishkumar, A.; Kumaresan, V.; Velraj, R., Solidification characteristics of water based graphene nanofluid PCM in a spherical capsule for cool thermal energy storage applications. *International Journal of Refrigeration* **2016,** *66*, 73-83.

22. Liu, Y.; Li, X.; Hu, P.; Hu, G., Study on the supercooling degree and nucleation behavior of water-based graphene oxide nanofluids PCM. *International Journal of Refrigeration* **2015,** *50*, 80-86.

23. Ivall, J.; Hachem, M.; Coulombe, S.; Servio, P., Behavior of Surface-Functionalized Multiwall Carbon Nanotube Nanofluids during Phase Change from Liquid Water to Solid Ice. *Crystal Growth and Design* **2015,** *15* (8), 3969-3982.

24. Jin, Z.; Zhang, H.; Yang, Z., Experimental investigation of the impact and freezing processes of a water droplet on an ice surface. *International Journal of Heat and Mass Transfer* **2017,** *109*, 716-724.

25. Walford, M. E. R.; Hargreaves, D. M.; Stuart-Smith, S.; Lowson, M., Freezing of water drops on a cold surface. *Journal of Glaciology* **1991,** *37* (125), 47-50.

26. Sanz, A.; Meseguer, J.; Mayo, L., The influence of gravity on the solidification of a drop. *Journal of Crystal Growth* **1987,** *82* (1), 81-88.

27. Snoeijer, J. H.; Brunet, P., Pointy ice-drops: How water freezes into a singular shape. *American Journal of Physics* **2012,** *80* (9), 764-771.

28. Carte, A. E., Air Bubbles in Ice. *Proceedings of the Physical Society* **1961,** *77* (3), 757-768.

29. Chu, F.; Zhang, X.; Li, S.; Jin, H.; Zhang, J.; Wu, X.; Wen, D., Bubble formation in freezing droplets. *Physical Review Fluids* **2019,** *4* (7), 071601.

30. Chaudhary, G.; Li, R., Freezing of water droplets on solid surfaces: An experimental and numerical study. *Experimental Thermal and Fluid Science* **2014,** *57*, 86-93.

31. Callister, W. D.; Rethwisch, D. G., *Materials Science and Engineering: An Introduction*. 8 ed.; John Wiley and Sons, Inc.: Hoboken, NJ, 2010.

32. Korayem, A. H.; Tourani, N.; Zakertabrizi, M.; Sabziparvar, A. M.; Duan, W. H., A review of dispersion of nanoparticles in cementitious matrices: Nanoparticle geometry perspective. *Construction and Building Materials* **2017,** *153*, 346-357.

33. Hemmingsen, E., Permeation of Gases through Ice. *Tellus* **1959,** *11* (3), 355-359.

34. Hallett, J., Experimental Studies of the Crystallization of Supercooled Water. *Journal of Atmospheric Sciences* **1964,** *21*, 671-682.

35. Peppin, S. S.; Wettlaufer, J. S.; Worster, M. G., Experimental verification of morphological instability in freezing aqueous colloidal suspensions. *Physical review letters* **2008,** *100* (23), 238301.

36. Petrenko, V. F.; Whitworth, R. W., *Physics of Ice*. Oxford University Press: Oxford, 2002; p 392.

37. You, J.; Wang, L.; Wang, Z.; Li, J.; Wang, J.; Lin, X.; Huang, W., Interfacial undercooling in solidification of colloidal suspensions: analyses with quantitative measurements. *Sci Rep* **2016,** *6*, 28434.

38. Peppin, S. S. L.; Worster, M. G.; Wettlaufer, J. S., Morphological instability in freezing colloidal suspensions. *Proceedings of the Royal Society A: Mathematical, Physical and Engineering Sciences* **2007,** *463* (2079), 723-733.

39. Agaliotis, E.; Schvezov, C.; Rosenberger, M.; Ares, A., A numerical model study of the effect of interface shape on particle pushing. *Journal of Crystal Growth* **2012,** *354*, 49–56.

40. Kundin, J.; Aufgebauer, H.; Reimann, C.; Seebeck, J.; Friedrich, J.; Jauss, T.; Sorgenfrei, T.; Croell, A., Dynamic Modeling of Critical Velocities for the Pushing/Engulfment Transition in the Si-SiC System Under Gravity Conditions. *Metallurgical and Materials Transactions A* **2017,** *48* (1), 342-353.

41. Tao, Y.; Yeckel, A.; Derby, J. J., Steady-state and dynamic models for particle engulfment during solidification. *Journal of Computational Physics* **2016,** *315*, 238-263.

42. Jia, L.; Chen, Y.; Lei, S.; Mo, S.; Luo, X.; Shao, X., External electromagnetic field-aided freezing of CMC-modified graphene/water nanofluid. *Applied Energy* **2016,** *162*, 1670-1677.

43. Pötschke, J.; Rogge, V., On the behaviour of foreign particles at an advancing solid-liquid interface. *Journal of Crystal Growth* **1989,** *94* (3), 726-738.

44. Field, P. R.; Lawson, R. P.; Brown, P. R. A.; Lloyd, G.; Westbrook, C.; Moisseev, D.; Miltenberger, A.; Nenes, A.; Blyth, A.; Choularton, T.; Connolly, P.; Buehl, J.; Crosier, J.; Cui, Z.; Dearden, C.; DeMott, P.; Flossmann, A.; Heymsfield, A.; Huang, Y.; Kalesse, H.; Kanji, Z. A.; Korolev, A.; Kirchgaessner, A.; Lasher-Trapp, S.; Leisner, T.; McFarquhar, G.; Phillips, V.; Stith, J.; Sullivan, S., Secondary Ice Production: Current State of the Science and Recommendations for the Future. *Meteorological Monographs* **2017,** *58*, 7.1-7.20.

45. Borode, A. O.; Ahmed, N. A.; Olubambi, P. A., Surfactant-aided dispersion of carbon nanomaterials in aqueous solution. *Physics of Fluids* **2019,** *31* (7), 071301.

46. Amrollahi, A.; Hamidi, A. A.; Rashidi, A. M., The effects of temperature, volume fraction and vibration time on the thermo-physical properties of a carbon nanotube suspension (carbon nanofluid). *Nanotechnology* **2008,** *19* (31), 315701.

47. Chang, R., *Physical chemistry for the chemical and biological sciences*. University Science Books: 2000.